PHYSICAL REVIEW C **71**, 064311 (2005)

Investigation of ^{6}He cluster structures

L. Giot,*,† P. Roussel-Chomaz, C. E. Demonchy, W. Mittig, and H. Savajols
GANIL, BP 5027, F-14076 Caen, France

N. Alamanos, F. Auger, A. Gillibert, C. Jouanne, V. Lapoux,
L. Nalpas, E. C. Pollacco, J. L. Sida, and F. Skaza
DSM/Dapnia CEA Saclay, F-91191 Gif-sur-Yvette, France

M. D. Cortina-Gil and J. Fernandez-Vasquez
Universidad de Santiago de Compostela,
E-15706 Santiago de Compostela, Spain

R. S. Mackintosh
Department of Physics and Astronomy, The Open University,
Milton Keynes, MK7 6AA, United Kingdom

A. Pakou
University of Ioannina, GR-45110 Ioannina, Greece

S. Pita
APC, 11 place Marcelin Berthelot, F-75231 Paris, France

A. Rodin, S. Stepantsov, and G. M. Ter Akopian
Flerov Laboratory of Nuclear Reactions, JINR, Dubna RU-141980, Russia

K. Rusek
Department of Nuclear Reactions, The Andrzej Soltan Institute for Nuclear Studies,
Hoza 69, PL-00-681 Warsaw, Poland

I. J. Thompson
University of Surrey, Guildford, GU2 7XH, United Kingdom

R. Wolski
The Henryk Niewodniczański Institute of Nuclear Physics PAN,
Radzikowskiego 152, PL-31-342 Cracow, Poland
(Received 16 January 2005; published 23 June 2005)

The α+2n and t+t clustering of the ^{6}He ground state were investigated by means of the transfer reaction ^{6}He(p, t)^{4}He at 25 MeV/nucleon. The experiment was performed in inverse kinematics at GANIL with the SPEG spectrometer coupled to the MUST array. Experimental data for the transfer reaction were analyzed by a distorted wave Born approximation (DWBA) calculation, including the two neutrons and the triton transfer. The couplings to the $^6\text{He} \rightarrow {}^4\text{He} + 2n$ breakup channels were taken into account with a polarization potential deduced from a coupled-discretized-continuum channels analysis of the $^6\text{He} + {}^1\text{H}$ elastic scattering measured at the same time. The influence on the calculations of the α+t exit potential and of the triton sequential transfer is discussed. The final calculation gives a spectroscopic factor close to one for the α+2n configuration as expected. The spectroscopic factor obtained for the t+t configuration is much smaller than the theoretical predictions.

DOI: 10.1103/PhysRevC.71.064311 PACS number(s): 25.60.−t, 24.10.Eq, 27.20.+n, 21.10.Jx

I. INTRODUCTION

In the vicinity of the neutron drip line, the weak binding of the nuclei leads to exotic features such as halos [1]. Furthermore, the two neutrons halo systems, such as ^{6}He, ^{11}Li, and ^{14}Be, exhibit Borromean characteristics, whereby the two-body subsystems are unbound [2]. Among these

*Present address: GSI, Planckstr.1, D-64291 Darmstadt, Germany.
†Electronic address: l.giot@gsi.de

Borromean nuclei, the case of the ^{6}He nucleus is of a special interest from both experimental and theoretical points of view to study the halo phenomenon and three-body correlations, especially because the α core can be represented as structureless. The importance of the di-neutron and cigarlike $\alpha+2n$ configurations predicted for the ^{6}He ground-state wave function [2] was investigated by means of a $2n$ transfer reaction or a radiative proton capture [3,4]. These two experiments give opposite conclusions concerning the relative importance of di-neutron and cigarlike configurations.

An additional question arises whether the only contributions to the ^{6}He ground-state wave function are the cigar and di-neutron configurations or if some $t+t$ clustering is also present. According to translational invariant shell-model calculations [5], the ^{6}He nucleus is expected to have a large spectroscopic amplitude for the $t+t$ configuration as well as for the $\alpha+2n$ configuration, such as ^{6}Li nucleus for the configurations $\alpha+d$ and ^{3}He$+t$. Microscopic multicluster calculations show also that the binding energy of ^{6}He is better reproduced by including some $t+t$ clustering in the ground-state wave function [6]. The spectroscopic factors predicted for the $t+t$ configuration by the different models range from 0.44 [7] to 1.77 [5].

Experimentally, this $t+t$ clustering was investigated for the first time by means of (t,^{6}He) transfer reactions on several targets and a spectroscopic factor S_{t-t} of 1.77 was proposed [8]. Recently, Wang *et al.* determined the charge radius of the ^{6}He nucleus by using a laser spectroscopy method and compared the experimental extracted radius with those predicted by nuclear structure calculations [9]. The experimental radius is very close to the predictions of the $\alpha+2n$ cluster models but far away from those using a combination of $\alpha+2n$ and $t+t$ clusters. To determine the importance of the $\alpha+2n$ and $t+t$ configurations of the ^{6}He nucleus, Wolski *et al.* measured at Dubna the intermediate angles of the ^{6}He$(p,t)^4$He angular distribution [10], in analogy with the reaction ^{6}Li$(p,^3$He$)^4$He used to study the relative importance of the configurations $\alpha+d$ and ^{3}He$+t$ for the ^{6}Li nucleus [11]. This reaction performed at 150 MeV can proceed as the transfer of two neutrons or of a ^{3}H from the ^{6}He nucleus. Several analyses leading to very different spectroscopic factors S_{t-t} were performed on these experimental data within the distorted wave Born approximation (DWBA) framework. The DWBA analysis done by Wolski *et al.* suggests a spectroscopic factor S_{t-t} of 0.42. Rusek *et al.* also conclude to a small spectroscopic factor S_{t-t} equal to 0.25 [12]. The extreme case is the analysis of Oganessian *et al.*, which described the data in a four-body three-dimensional DWBA approach without any $t+t$ clustering [13]. At the opposite, Heiberg-Andersen *et al.* reproduced these data with a spectroscopic factor S_{t-t} of 1.21 and took also into account the $2n$ sequential transfer [14]. All these calculations call for data covering a wider range, especially at backward angles where the dependence of the ^{6}He$(p,t)^4$He differential cross section with the value of the spectroscopic factor S_{t-t} is important, whereas the effect of the spectroscopic factor $S_{\alpha-2n}$ is dominant at forward angles. Hence to clarify the situation between the different values of the spectroscopic factor S_{t-t}, we measured at GANIL the complete angular distribution for the ^{6}He$(p,t)^4$He with a special emphasis on the forward and backward angles that were never measured.

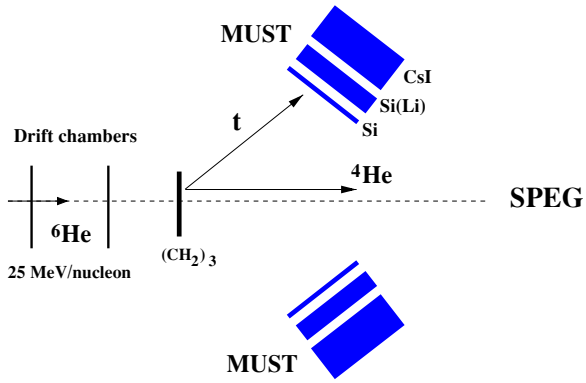

FIG. 1. (Color online) Experimental setup.

II. EXPERIMENTAL METHOD

The experiment was carried out at the GANIL coupled cyclotron facility. The composite secondary beam was produced by the fragmentation of a 780 MeV ^{13}C beam of 5 μAe on a 1040 mg/cm^2 carbon production target located between the two superconducting solenoids of the SISSI device [15]. The ^{6}He nuclei were selected with the two dipoles of the α spectrometer and an achromatic Al degrader located at the dispersive plane between these two dipoles. The only contaminant was ^{9}Be at a level of 1%. The resulting 150 MeV ^{6}He beam with an average intensity of 1.1×10^5 pps impinged on a $(CH_2)_3$ target, 18 mg/cm^2 thick, located in the reaction chamber. A sketch of the experimental setup is shown on Fig. 1. Due to the large emittance of the secondary fragmentation beam, the incident angle and the position on the target of the nuclei were monitored event by event by two low pressure drift chambers [16]. The angular and position resolutions on the target were respectively 0.14° and 2.4 mm.

The ^{4}He and ^{3}H from the ^{6}He$(p,t)^4$He reaction for center-of-mass angles between 20° and 110° were detected in coincidence by the eight telescopes of MUST silicon detector array [17]. These detectors were separated in two groups arranged to form two 12×12 cm^2 squares placed on each side of the beam, one covering an angular range between 6° and 24° and the other one between 20° and 38° with respect to the beam direction. The angular coverage in the vertical direction was ±9°. Each of the MUST telescopes is composed of a doubled-sided silicon strip detector backed by a Si(Li) and a CsI scintillator, which provide an energy measurement. The silicon strip detector is 300 μm thick with 60 strips (1 mm wide) on each side and provides X-Y position measurement, from which the scattering angle is determined. The energy resolution in the silicon strips detectors was 65 keV and the angular resolution 0.15°. The ^{4}He and ^{3}H nuclei were identified by the standard ΔE-E technique. Due to a saturation of the Si(Li) preamplifiers, we did not measure the total energy of the α particles. The offline identification combined with a

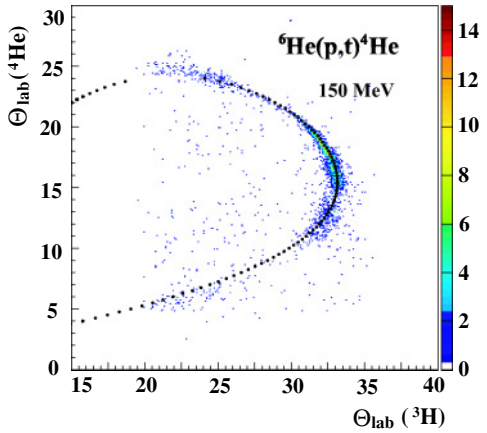

FIG. 2. (Color online) Scatterplot of the ^{4}He laboratory angle versus the ^{3}H laboratory angle detected in coincidence in the MUST array for the ^{6}He$(p, t)^4$He reaction.

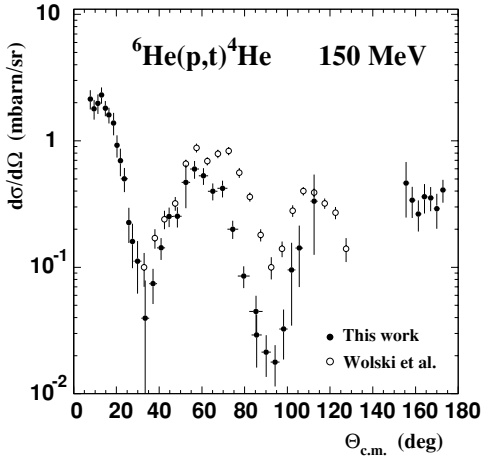

FIG. 3. Differential cross section for the ^{6}He$(p, t)^4$He reaction. The full circles correspond to the present data. The open circles are the data measured at Dubna [10].

gate on the kinematical locus of the transfer reaction on the ^{3}H plot, energy versus scattering angle, reduced the background from the carbon component of the target. Figure 2 shows the angular correlation of the ^{4}He and ^{3}H nuclei. The dotted line corresponds to the calculated two-body kinematical line for the (p, t) transfer reaction toward the ^{6}He ground state. The remaining backgound in the vicinity of this line was evaluated and subtracted to the region of interest.

The forward and backward center-of-mass (c.m.) angles of the angular distribution for the ^{6}He$(p, t)^4$He reaction were measured with the SPEG spectrometer [18] by detecting respectively the high-energy ^{4}He and the high-energy triton at forward laboratory angles. The particles were identified in the focal plane by the energy loss measured in an ionization chamber and the residual energy measured in plastic scintillators. The momentum and the scattering angle were obtained by track reconstruction of the trajectory as determined by two drift chambers located near the focal plane of the spectrometer. The spectrometer was also used to measure the elastic scattering ^{6}He$(p, p)^6$He angular distribution from 14° c.m. to 60° c.m.

To extract differential cross sections, data were corrected for the geometrical efficiency of the detection in SPEG or MUST. This efficiency was determined through a Monte Carlo simulation whose ingredients are the detector geometry, their experimental angular and energy resolutions, the position and the width of the beam on the target. The error on the MUST detection efficiency deduced from the Monte Carlo simulation is estimated to be 5%. The absolute normalization for the elastic scattering data on the protons in the $(CH_2)_3$ target and for the transfer reaction was obtained from the elastic scattering on ^{12}C, which was measured simultaneously. Elastic scattering calculations for the system ^{6}He+^{12}C using different optical potentials [19,20] show that the angular distribution at forward angles up to 7° c.m. is dominated by Coulomb scattering and is rather insensitive to the potential used. Therefore the absolute normalization of the data was obtained from the measured cross section on the first maximum of the ^{6}He(^{12}C,^{12}C)^{6}He angular distribution. The uncertainty on the normalization is of the order of 10%. The same normalization factor was applied to the transfer data measured with the SPEG spectrometer. In the overlap domain between 19° c.m. and 27° c.m. for the transfer data obtained with SPEG or MUST, the agreement was good. The final differential cross section in this angular region is the statistical average value between the two sets of data. Figure 3 displays the transfer data obtained in the present experiment together with results measured previously at Dubna at the same energy [10]. The uncertainty of the dubna differential cross sections is estimated to be within a 30% limit, mainly because of the beam monitoring errors. The error bars displayed for the GANIL data are purely statistical. The data points between 120° and 155° could not be obtained because of a lack of statistics in a set of runs with the MUST array positionned in this angular region. The main difference between the two sets of data obtained at GANIL and Dubna is related to the width of the second minimum around 90°, which is larger in our case. The Dubna data were extracted from the energy correlation between the α particles and the tritons detected in coincidence in two telescopes. This energy correlation presented a strong background, caused by the breakup of the ^{6}He particles on the carbon component of the target. The breakup background is not uniform and could explain the difference observed between the two sets of data in the angular range corresponding to the deep minimum around 90°. Here, the angular correlation of the ^{4}He and ^{3}H nuclei combined with a selection on the kinematical locus on the ^{3}H plot, energy versus scattering angle, reduced strongly the breakup background and improved the quality of the data, as shown on Fig. 2. Moreover, the oscillation widths of the GANIL data are in better agreement with the new data measured at Dubna by Stepantsov *et al*. [21].

III. ELASTIC SCATTERING AND THE ^{6}He+p OPTICAL POTENTIAL

The ^{6}He+p elastic scattering data obtained here complement the data measured at Dubna at the same energy in two differents runs [10,22]. Figure 4 shows the three sets of

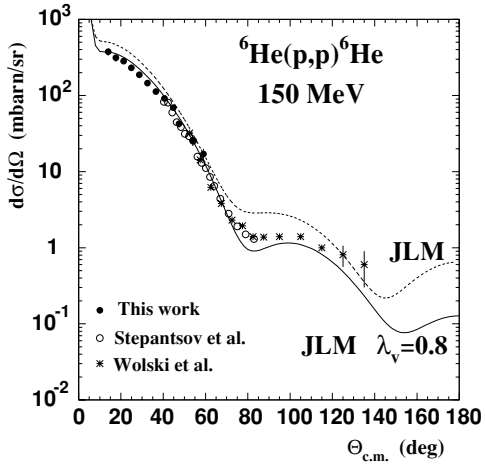

FIG. 4. Differential cross section for the ^{6}He$(p,p)^6$He elastic scattering compared to JLM calculations. The full circles correspond to the present data. The open circles and the crosses are the data measured at Dubna [10,22].

data that are in excellent agreement. These new data allow to better determine the nuclear interaction potential ^{6}He+p, which is an essential ingredient for the analysis of the transfer reaction, because it is necessary for the entrance channel in the DWBA calculation. Previous results obtained on ^{6}He+p elastic scattering in the same energy range have shown that the nucleon-nucleus optical models potentials used for stable nuclei have to be modified in the case of loosely bound nuclei such as ^{6}He [12,23]. Coupling to the continuum and to the resonant states are expected to play a significant role because the scattering states are much closer to the continuum states than in stable nuclei. In this work, we tried two approaches to take into account these couplings to the continuum and thus the breakup effects. First, these effects were phenomenologically simulated by reducing the real part of the potential or by adding a dynamical polarization potential as discussed in Ref. [23]. In this case, the interaction potential ^{6}He+p was calculated within the approach derived by Jeukenne, Lejeune, and Mahaux (JLM) [24]. As seen in Fig. 4, this renormalization of the real part of the JLM potential allows also to reproduce the sets of data obtained at GANIL and Dubna reasonably well.

In a second approach, the coupling to the continuum was explicitly included by means of the coupled discretized continuum channels (CDCC) method. This approach previously used by Rusek *et al.* [12,25] assumes a two body cluster model α+2n for the ^{6}He nucleus with the spin of the 2n cluster set to $s=0$. The wave functions $\Psi_0(r)$ and $\Psi_2(r)$ describing the relative motion of the two clusters in the ^{6}He ground state and the ^{6}He(2^+) resonant state were calculated in potential wells whose depths were varied to reproduce respectively the binding energy of 0.975 MeV and the excitation energy of 1.8 MeV. The parameters of these Woods-Saxon binding potentials are listed in Table I. The continuum above the $^6\text{He} \rightarrow \alpha + 2n$ breakup threshold was discretized into a series of momentum bins with respect to the relative α-2n momentum k. The lowest bins were of $\Delta k = 0.25$ fm^{-1}, whereas all the others were of $\Delta k = 0.2$ fm^{-1}. The model space was truncated at the energies close to the t+t breakup threshold. The wave function $\Psi(r)$ representing a bin is the average function over the bin width of the cluster wave functions $\phi(r,k)$ in the bin,

$$\Psi(r) = \frac{1}{\sqrt{N\Delta k}} \int_{\Delta k} \phi(r,k) dk, \tag{1}$$

where r is the ^{4}He-2n distance and N is the normalization factor. All the spectroscopic amplitudes for the couplings are assumed to be equal to 1. The central and coupling potentials $V_{i\rightarrow f}(R)$ used in the CDCC calculations were derived from ^{4}He$-p$ and 2n–p potentials by means of the single-folding method,

$$V_{i\rightarrow f}(R) = \langle \Psi_f(r) | U_{2n-p}(|\vec{R} + 2/3\vec{r}|) + U_{^4\text{He}-p}(|\vec{R} - 1/3\vec{r}|) | \Psi_i(r) \rangle, \tag{2}$$

where R is the distance between the ^{6}He nucleus and the proton. The $2n-p$ potential was assumed to be the same as for d-p. The parameters of the optical potentials U_{2n-p} and $U_{^4\text{He}-p}$, listed in Table II, were obtained by fitting the elastic scattering data of deuterons and alpha particles from protons at the required energy [26,27]. The results of the CDCC calculations for the ^{6}He+p elastic scattering, performed using version FRXY-1c of the code FRESCO [28], are plotted in Fig. 5 together with the three sets of data measured at GANIL and Dubna.

These CDCC calculations reproduce, too, the values and the slope of the differential cross section for the inelastic scattering exciting ^{6}He to its 2^+ resonant state [22]. The calculated value of the reduced transition probability $B(E2; \text{g.s.} \rightarrow 2^+) = 7.08\, e^2$ fm^4 is larger than the value of 3.21 e^2 fm^4 published earlier by Aumann *et al.* [29]. However, it should be noticed that the determination of $B(E2)$ is strongly model dependent when the reaction is not dominated by the Coulomb interaction.

TABLE I. Parameters of the binding potentials and the spectroscopic amplitudes.

	V_0 (MeV)	R_0 (fm)	a_0 (fm)	Ref.	S_a	Ref.
$^6\text{He}_{\text{g.s.}} = \alpha + 2n$	69.393	1.9	0.65	[25]	1.	This work
$^6\text{He}_{2+} = \alpha + 2n$	80.427	1.9	0.65	[25]	1.	[25]
$^6\text{He}_{\text{g.s.}} = t + t$	80.	1.9	0.65	[8]	−0.28	This work
$^3\text{H}_{\text{g.s.}} = p + 2n$	44.382	2.	0.60	[34]	1.	[38]
$^4\text{He}_{\text{g.s.}} = p + t$	61.4	2.	0.60	[34]	1.4142	[38]
$^4\text{He}_{\text{g.s.}} = ^3\text{He} + n$	61.4	1.5	0.40	This work	−1.4142	[38]

TABLE II. Parameters of the input optical model potentials.

	V_0 (MeV)	R_0 (fm)	a_0 (fm)	W_v (MeV)	R_v (fm)	a_v (fm)	W_s (MeV)	R_s (fm)	a_s (fm)	Ref.
$d+p$	65.80	1.25	0.501	0.00	0.00	0.00	10.00	1.20	0.517	[12]
^{3}He + ^{3}He	60.00	2.58	0.417	0.00	0.00	0.00	0.00	0.00	0.00	This work
$\alpha+p$	48.90	1.75	0.477	0.557	1.75	0.477	0.00	0.00	0.00	This work
$\alpha+^3$He, Pot. A	80.95	2.39	0.829	7.49	4.12	0.0196	0.00	0.00	0.00	This work
$\alpha+^3$He, Pot. B	142.92	2.57	0.271	0.86	6.88	0.972	0.00	0.00	0.00	[12]

In particular, the value of $B(E2)$ depends on the choice of the neutron density distribution.

By inversion from the elastic channel S matrix, generated by the CDCC calculations, a local potential ^{6}He+p, including the breakup effects, is obtained. The inversion is carried out using the iterative-perturbative (IP) method [30,31]. The angular distribution calculated within the CDCC approach or with the local potential, named Pot. IP, can hardly be distinguished in Fig. 5. The reaction cross sections calculated respectively with the potential IP and the renormalized JLM potential are respectively $\sigma_R = 532$ mb and 394 mb. The reaction cross section for ^{6}He on proton has been measured at 36 MeV/nucleon using the transmission method and a value of $\sigma_R = 409 \pm 22$ mb was obtained [32]. Considering that in the present energy domain, the reaction cross section σ_R increases when the energy of the projectile decreases [33], the experimental value at 25 MeV/nucleon should be closer to the value calculated with the IP potential. This IP local potential and the renormalized JLM potential will be tested in the next section as entrance potentials for the DWBA calculations, of the ^{6}He$(p, t)^4$He.

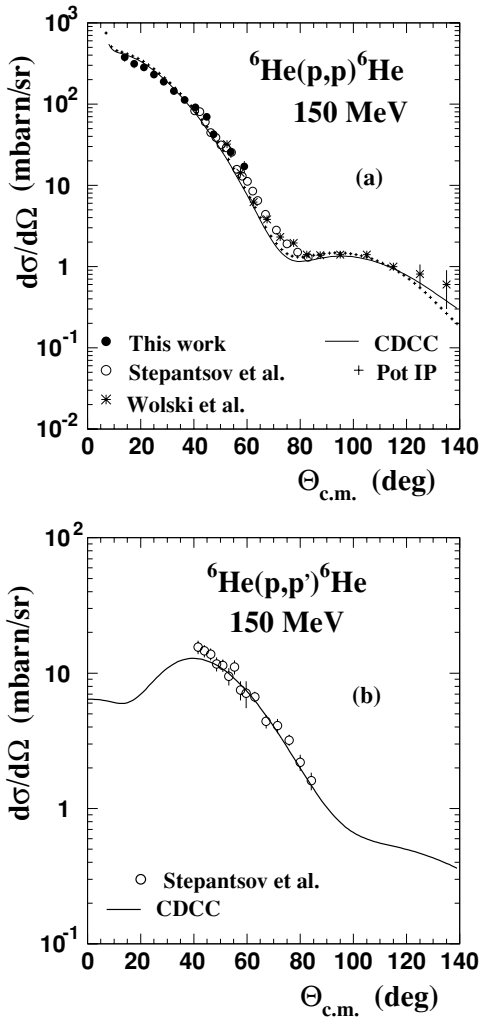

FIG. 5. (a) CDCC calculations for the elastic scattering of ^{6}He from ^{1}H. The experimental data are from this work (black circles) and from Ref. [10,22]. (b) CDCC calculations for the inelastic scattering of ^{6}He from ^{1}H leading to the 2^+ resonant state of ^{6}He at excitation energy of 1.8 MeV. The experimental data are from Ref. [22].

IV. DWBA ANALYSIS OF ^{6}He$(p, t)^4$He

DWBA calculations including both $2n$ and t transfer from the ^{6}He ground state, were performed on the ^{6}He$(p, t)^4$He data with the code FRESCO used in its finite range option. A sketch of the calculation is shown in Fig. 6. The couplings to the continuum states were taken into account with the entrance channel potential ^{6}He+p calculated, as described above within the JLM or the CDCC framework. The effect of the triton sequential transfer ($t = 2n + p$) was also investigated. The wave functions describing the relative motion of the two clusters α+$2n$, t+t, p+t, and p+$2n$ respectively in the ground state of ^{6}He, ^{4}He, and ^{3}H were obtained from Woods-Saxon potentials with the well depth adjusted to reproduce the corresponding binding energies, according to the usual separation energy prescription. The remnant potential V_{p-t}

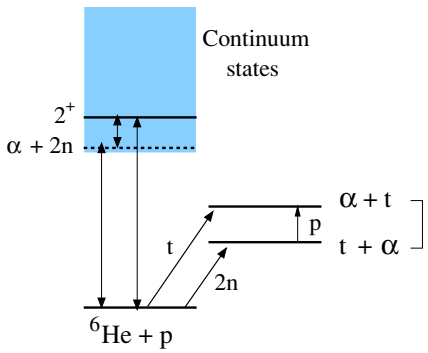

FIG. 6. (Color online) Scheme of the ^{6}He$(p, t)^4$He DWBA calculation.

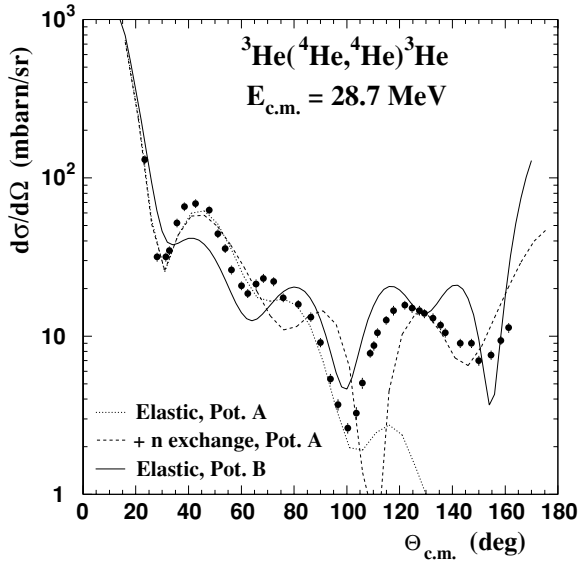

FIG. 7. Differential cross section for the ^{3}He(α, α)^{3}He reaction compared with DWBA calculations assuming only the elastic scattering and after the one neutron exchange. The experimental data are from Schwandt *et al*. [37].

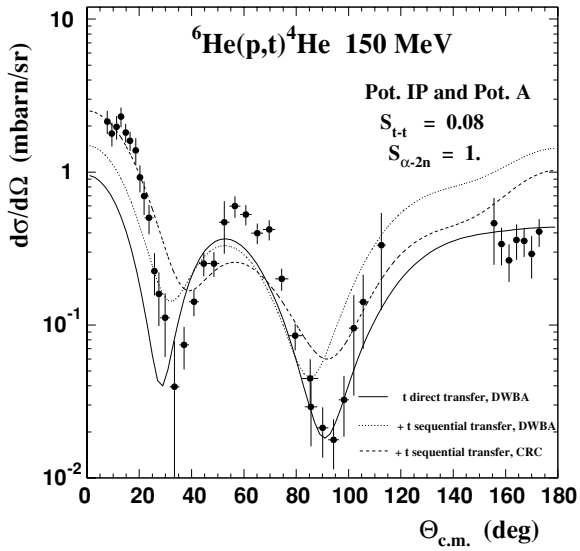

FIG. 8. Effect of the sequential transfer of the triton ($t = 2n + p$) on the ^{6}He(p, t)^{4}He reaction.

was taken from Ref. [34] and the remnant potential $V_{\alpha-p}$ was determined in the previous section. All the potentials and the spectroscopic amplitudes used in the calculation are listed in Tables I and II.

Special care was taken in the choice of the potential for the $\alpha+t$ exit channel and several potentials were considered [10,12,13,34–36]. To obtain the $\alpha+t$ potential, we used $\alpha+^3$He elastic-scattering data at E$_{c.m.}$ = 28.7 MeV [37] as the ^{3}H(α, α)^{3}H reaction was not studied in the energy range considered presently. Two approaches were considered to extract the $\alpha+^3$He optical potential. The process of one neutron transfer, which is not distinguishable experimentally from the elastic scattering, was first explicitly taken into account in a DWBA analysis of the ^{3}He(α, α)^{3}He reaction. The dotted and dashed curves on Fig. 7 show respectively the contribution of the elastic scattering and the one neutron exchange to the ^{3}He(α, α)^{3}He reaction. Hence, the potential A extracted from the DWBA analysis represents only the elastic scattering between the α and the ^{3}He. Next, we used the potential B obtained in Ref. [12] fitted on the complete differential cross section of the ^{3}He(^{4}He,^{4}He)^{3}He elastic scattering. This fit on the $\alpha+^3$He data corresponds to the solid line on Fig. 7. Although the fit is still far from perfect, it reproduces the gross features of the measured angular distribution. The values of these two exit potentials A and B are given in Table II.

Both the direct and the sequential transfer of the triton were included in a DWBA calculation, described on Fig. 6, and then in a coupled reaction channels calculation (CRC) where the backcouplings were taken into account. The proton transfer, which is the second step of the triton sequential transfer, can be seen as a proton exchange between the two exit channels ^{3}H+α and $\alpha+^3$H and is directly included in the DWBA calculation. Hence, the exit channel potential $\alpha+^3$H has not to take into account the proton exchange but only the elastic scattering. This corresponds to the potential A, as determined above, for the exit channel. A comparison between a DWBA calculation with only the triton direct transfer and DWBA and CRC calculations, including the sequential transfer $t = 2n + p$, is shown on Fig. 8. These calculations do not allow to reproduce at the same time the experimental data at forward and backward angles. Futhermore, the amplitude and/or the position of the oscillation at 60° is not reproduced.

Hence, we used Potential B for the exit channel of the reaction, considering that the proton exchange in the $\alpha+t$ partition, and consequently the sequential triton transfer, could be in some sense described by the exchange term included in the Potential B. Only the $2n$ and the direct triton transfer are thus explicitly included in the DWBA calculation. Figure 9

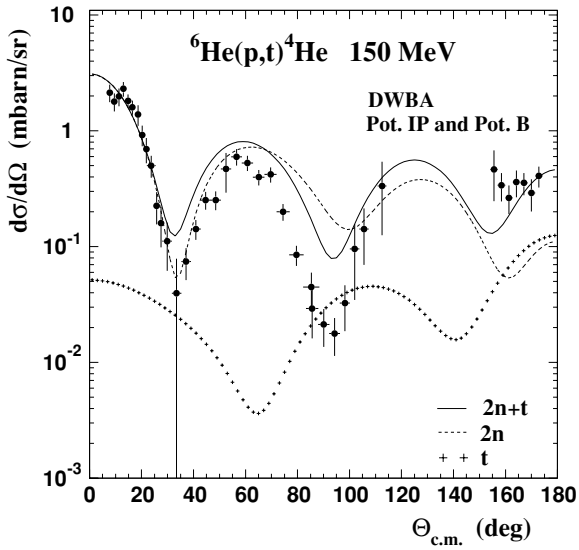

FIG. 9. Contributions of $2n$ and t transfer to the DWBA calculation of ^{6}He(p, t)^{4}He.

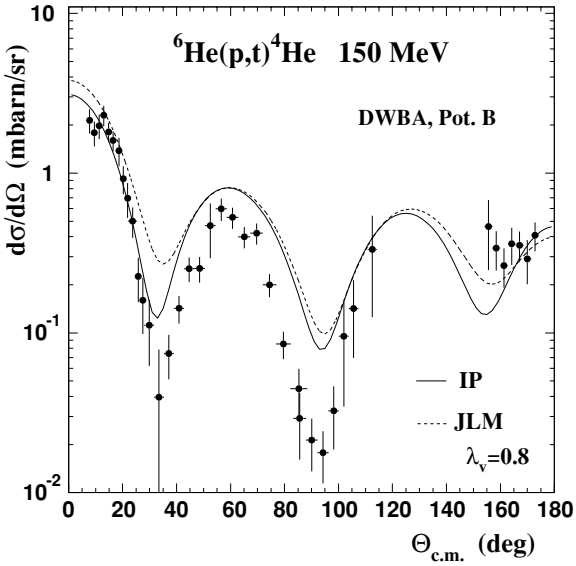

FIG. 10. Dependence of the results of the DWBA calculation on the choice of the ^{6}He+p entrance potential.

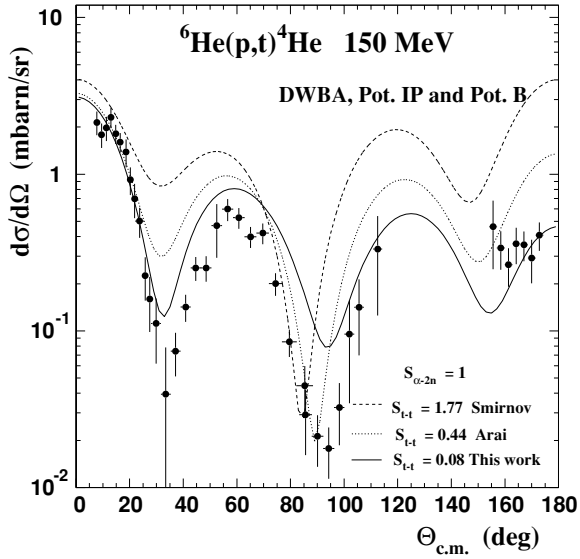

FIG. 11. Dependence of the DWBA calculation with the value of the spectroscopic factor S_{t-t}.

compares the ^{6}He(p, t)^{4}He differential cross section obtained at GANIL with the DWBA calculation using Potential IP for the entrance channel and Potential B for the exit channel, which gives actually the best description of the features of the ^{6}He(p, t)^{4}He angular distribution. The spectroscopic factors for the α+2n and t+t configurations were adjusted to reproduce the data. The adjustment on Fig. 9 is a compromise between the experimental values at forward and backward angles and the width of the second oscillation. The dashed line on Fig. 9 corresponds to the DWBA calculation where only the 2n transfer is taken into account with a spectroscopic factor $S_{\alpha-2n}$ equal to 1, which is close to the predicted value [38]. The spectroscopic factor S_{t-t}, determined from the comparison with the data at backward angles, is equal to 0.08 with an uncertainty of the order of 50%. The crosses on Fig. 9 correspond only to the triton transfer. The solid line is the coherent sum of the two processes with these values of their spectroscopic factors. Even if the spectroscopic factor of the t+t clustering is small, the $t-t$ component is essential to reproduce the backward angles.

We tried to include the sequential transfer of the two neutrons, processing via the ^{5}He+d channel. This calculation required the optical potential for the ^{5}He+d system. Of course, no deuton elastic scattering data exist for this unbound nucleus. A first potential was obtained from the ^{6}He(p, d)^{5}He reaction [10]. The second potential was calculated from a method proposed by Keaton *et al.* convoluting the potentials ^{5}He+p and ^{5}He+n, derived from the CH89 parametrization, with a deuteron wave function [39–41]. These two potentials provided a very poor reproduction for the one- and two-neutron transfer reactions. Therefore, we removed this channel in the final caculation, because of the lack of a reliable potential for the unbound nucleus ^{5}He.

Finally, both entrance potentials including breakup effects, obtained in the previous section, were also tested in Fig. 10. Obviously, the IP potential deduced from a coupled-discretized-continuum-channels calculation, where the couplings to the continuum are explicitly taken into account, improves the description of the data compared to the JLM approach.

Figure 11 shows the dependence of the DWBA calculation with the value of the spectroscopic factor S_{t-t} for three cases: (*i*) the value derived from the present work, (*ii*) the value obtained in the three-body cluster model by Arai *et al.* [7], and (*iii*) finally the value from a translational invariant shell-model calculation [5]. It is clear that in the present analysis, the two last values strongly overestimate the cross section measured at backward angles, and that the largest value even affects the reproduction of the most forward angles of the data. The theoretical values are considerably outside the range of the uncertainty of the experimental data. The different approaches of analysis performed within this work showed that the final results somewhat depend on the potentials used in the calculation, especially in the exit channel potential. Considering the difficulties mentioned previously on this potential, one cannot exclude that another type of approach used to derive this potential could alter our conclusion.

V. CONCLUSIONS

The ^{6}He(p, t)^{4}He reaction at 150 MeV has been investigated at GANIL to provide insight on the ^{6}He cluster structure: the α+2n and t+t configurations. The transfer differential cross section were measured with the SPEG spectrometer coupled to the MUST array. The transfer data obtained at forward and backward angles allowed determination of the spectroscopic factors $S_{\alpha-2n}$ and S_{t-t} and thus the contribution of the configurations α+2n and t+t to the ^{6}He ground-state wave function. The ^{6}He(p, t)^{4}He data were analyzed by means of the DWBA and the coupled channels method taking into account the direct 2n, the direct triton transfer, and also the sequential transfer of the triton. The ^{6}He+p entrance

channel optical potential of these calculations was obtained by the inversion of the elastic channel S matrix generated from a CDCC calculation that took into account all the couplings to the continuum states. This CDCC calculation, where the continuum above the $\alpha+2n$ threshold is discretized, reproduced the elastic ^{6}He$(p,p)^6$He, also measured in this experiment, and the ^{6}He$(p,p')^6$He inelastic data available at the same energy as the transfer reaction. A detailed study of the exit channel was performed. The difficulties encountered in this part of the analysis are related to the lack of ^{4}He$+t$ elastic scattering data in the energy range considered presently and to the strong effects of the neutron exchange in the ^{4}He$+^3$He system that was used instead. The best description of the experimental data was obtained with a DWBA calculation taking into account the $2n$ and t direct transfer. The triton sequential transfer is assumed to be directly included in the exchange term of the exit potential $\alpha+^3$H. The present work shows that the DWBA analysis of the transfer data is strongly dependent on the chosen potentials. Nethertheless, the transfer data at backward angles can be reproduced only with a spectroscopic factor S_{t-t} that is much smaller than the theoretical values and the $t-t$ configuration is necessary for the description of the ^{6}He ground-state wave function.

ACKNOWLEDGMENTS

The support provided by the SPEG staff of GANIL during the experiment is gratefully acknowledged. We thank Y. Blumenfeld and N. K. Timofeyuk for fruitful discussions during the course of this work. This work was financially supported by the IN2P3-Poland cooperation agreement 02–106. Additional support from the Human Potential Part of the FP5 European Community Programme (Contract No HPMT-CT-2000–00180) is also acknowledged.

[1] P. G. Hansen, A. S. Jensen, and B. Jonson, Annu. Rev. Nucl. Part. Sci. **45**, 591 (1995).
[2] M. V. Zhukov, B. V. Danilin, D. V. Fedorov, J. M. Bang, I. J. Thompson, and J. S. Vaagen, Phys. Rep. **231**, 151 (1993).
[3] G. M. Ter-Akopian *et al.*, Phys. Lett. **B426**, 251 (1998).
[4] E. Sauvan *et al.*, Phys. Rev. Lett. **87**, 042501 (2001).
[5] Yu. F. Smirnov and Yu. M. Tchuvil'sky, Phys. Rev. C **15**, 84 (1977).
[6] A. Csótó, Phys. Rev. C **48**, 165 (1993).
[7] K. Arai, Y. Suzuki, and R. G. Lovas, Phys. Rev. C **59**, 1432 (1999).
[8] N. M. Clarke, J. Phys. G **18**, 917 (1992).
[9] L. B. Wang *et al.*, Phys. Rev. Lett. **93**, 142501 (2004).
[10] R. Wolski *et al.*, Phys. Lett. **B467**, 8 (1999).
[11] M. F. Werby, M. B. Greenfield, K. W. Kemper, D. L. McShan, and Steve Edwards, Phys. Rev. C **8**, 106 (1973).
[12] K. Rusek, K. W. Kemper, and R. Wolski, Phys. Rev. C **64**, 044602 (2001).
[13] Yu. Ts. Oganessian, V. I. Zagrebaev, and J. S. Vaagen, Phys. Rev. C **60**, 044605 (1999).
[14] H. Heiberg-Andersen, J. S. Vaagen, and I. J. Thompson, Nucl. Phys. **A690**, 306c (2001).
[15] R. Anne, Nucl. Instrum. Methods B **126**, 279 (1997).
[16] M. Mac Cormick *et al.*, Rapport GANIL, No. R98-02, 1998.
[17] Y. Blumenfeld *et al.*, Nucl. Instrum. Methods A **421**, 471 (1999).
[18] L. Bianchi, B. Fernandez, J. Gastebois, A. Gillibert, W. Mittig, and J. Barette, Nucl. Instrum. Methods A **276**, 509 (1989).
[19] R. A. Broglia and A. Winther, *Heavy Ion Reactions*, (Benjamin/Cummings, New York, 1981), Vol. 1, p. 114.
[20] J. S. Al-Khalili *et al.*, Phys. Lett. **B378**, 45 (1996).
[21] S. V. Stepantsov, private communication.
[22] S. V. Stepantsov *et al.*, Phys. Lett. **B542**, 35 (2002).
[23] V. Lapoux *et al.*, Phys. Lett. **B517**, 18 (2001) and references therein.
[24] J.-P. Jeukenne, A. Lejeune, and C. Mahaux, Phys. Rev. C **16**, 80 (1977).
[25] K. Rusek and K. W. Kemper, Phys. Rev. C **61**, 034608 (2000).
[26] F. Hinterberger, G. Mairle, U. Schmidt-Rohr, G. J. Wagner, and P. Turek, Nucl. Phys. **A111**, 265 (1968).
[27] A. D. Bacher, G. R. Plattner, H. E. Conzett, D. J. Clark, H. Grunder, and W. F. Tivol, Phys. Rev. C **5**, 1147 (1972).
[28] I. J. Thompson, Comput. Phys. Rep. **7**, 167 (1988).
[29] T. Aumann *et al.*, Phys. Rev. C **59**, 1252 (1999).
[30] S. G. Cooper, V. I. Kukulin, R. S. Mackintosh, and V. N. Pomerantsev, Nucl. Phys. **A677**, 187 (2000).
[31] R. S. Mackintosh and K. Rusek, Phys. Rev. C **67**, 034607 (2003).
[32] A. de Vismes *et al.*, Phys. Lett. **B505**, 15 (2001).
[33] S. Kox *et al.*, Phys. Rev. C **35**, 1678 (1987).
[34] V. G. Neudatchin *et al.*, Lett. Nuovo Cimento **5**, 834 (1972).
[35] N. K. Timofeyuk, Phys. Rev. C **63**, 054609 (2001).
[36] B. Buck and A. C. Merchant, J. Phys. G **14**, L211 (1988).
[37] P. Schwandt, B. W. Ridley, S. Hayakawa, L. Put, and J. J. Kraushaar, Phys. Lett. **B30**, 30 (1969).
[38] O. F. Nemets *et al.*, Nucleon clusters in atomic nuclei and many-nucleon transfer reactions (in Russian), Appendix III, Ukrainian Academy of science, Institute for Nuclear Research, Kiev, 1998.
[39] P. W. Keaton, Jr., and D. D. Amstrong, Phys. Rev. C **8**, 1692 (1973).
[40] R. L. Varner, W. J. Thompson, T. L. MacAbee, E. J. Ludwig, and T. B. Clegg, Phys. Rep. **201**, 57 (1991).
[41] M. Lacombe, B. Loiseau, J. M. Richard, R. Vinh Mau, J. Côté, P. Pirès, and R. de Tourreil, Phys. Rev. C **21**, 861 (1980).